

# Phonon thermal transport in $\beta$ -NX (X=P, As, Sb) monolayers: A first-principles study

Armin Taheri, Carlos Da Silva, Cristina H. Amon

([armin.taheri@mail.utoronto.ca](mailto:armin.taheri@mail.utoronto.ca))

*Department of Mechanical and Industrial Engineering, University of Toronto,  
Ontario, Canada, M5S 3G8*

## Abstract

Thermal conductivity of novel  $\beta$ -NX (X=P, As, Sb) monolayers are explored using a first-principles density functional theory study based on the linearized Peierls-Boltzmann transport equation (PBTE). Our results show that room temperature thermal conductivity of  $\beta$ -NP,  $\beta$ -NAs, and  $\beta$ -NSb are about 1.1, 5.5, and 34.0 times higher than those of single elements  $\beta$ -P,  $\beta$ -As, and  $\beta$ -Sb monolayers, respectively. Analyzing phonon properties shows that higher phonon group velocities as well as phonon lifetimes are responsible for such an enhancement in lattice thermal conductivity of  $\beta$ -NX (X=P, As, Sb) binary alloys compared to single element group-VA monolayers. In addition, we find that  $\beta$ -NP has the minimum thermal conductivity between  $\beta$ -NX (X=P, As, Sb) monolayers, while it has the minimum average atomic mass. This is in contrast with usual expectation that lower mass systems have higher thermal conductivity. Based on our results, there is a competition between effects of harmonic and anharmonic phonon properties in determining the variation of thermal conductivity among  $\beta$ -NX (X=P, As, Sb) monolayers. Higher anharmonicity of  $\beta$ -NP is found to be responsible for lower thermal conductivity of this monolayer. Our findings show that a comprehensive understanding of both harmonic and anharmonic phonon properties is essential for thermal conductivity study in any system.

**Keywords:** Thermal conductivity, Density functional theory, Alloys, group-VA monolayers, Harmonic and anharmonic phonon properties

# 1-Introduction

Motivated by appealing electrical, optical, mechanical, and thermal properties of phosphorene (P) [1,2], two-dimensional (2D) nanostructures of group-VA (including P, As, Bi and Sb) have recently been brought into focus in the research community. As opposed to gapless graphene which has limited applications in semiconductor industry, 2D materials of group-VA show direct electronic band gap, up to about 2.62 eV [3]. In addition, members of this family possess superior electron carrier mobility that can be as high as about  $1000 \text{ cm}^2\text{V}^{-1}\text{s}^{-1}$  [3,4], which makes them potential candidates for application in next-generation circuits, electronic and optoelectronic devices. Having a variety of stable honeycomb allotropes, commonly named as  $\alpha$ -,  $\beta$ -,  $\gamma$ -, and  $\delta$ -phase is another distinguished feature of these monolayers [4–6]. The  $\beta$ -phase (buckled) and  $\alpha$ -phase (puckered) are generally the two most stable allotropes having the minimum average binding energy [4]. Theoretical and experimental studies have revealed that both of these phases can be synthesized using different methods such as mechanical exfoliation [7,8] or chemical vapor deposition (CVD) [9]. For instance, GaN(001) [10] can be used as substrates to synthesize stable layers of buckled phosphorene. From thermal point of view, their thermal conductivity monotonically decreases from about 110 W/mK to 4.0 W/mK as the atomic mass increases from P to Bi [11–14]. Thus, they can be categorized as relatively low thermal conductive nanosheets, making them promising for thermal management and thermoelectric applications. Based on the first-principles density functional theory (DFT) calculations and the full solution of the linearized Peierls-Boltzmann transport equation (PBTE), the room temperature (RT) thermal conductivity of  $\beta$ -P is reported to be 78 W/mK by Ref. [11] and 108.8 W/mK by Ref. [12]. Discrepancies can generally be attributed to different DFT settings and monolayer thickness adopted in the study.

Highly anisotropic and orthogonal thermal conductivity is a well-known property of  $\alpha$ -phase of group-VA monolayers, which stems from their anisotropic layered structure. The room temperature thermal conductivity of  $\alpha$ -P ( $\alpha$ -As) in zigzag direction is reported to be 110 (30.4) W/mK, almost three (four) times higher than its corresponding value in the armchair direction, 36 (7.8) W/mK [11,14]. Using the same methodology, values of about 65.4 W/mK [12], 13.8 W/mK [12], and 4.0 W/mK [13] are reported for thermal conductivity of  $\beta$ -As,  $\beta$ -Sb, and  $\beta$ -Bi at RT, respectively.

In addition to single element monolayers of group-VA, the recent emergence of their stable binary alloys with desirable electrical and thermal properties has opened up a broad avenue of photonic, nanoelectronic, optoelectronic, and thermoelectric applications [15,16]. A recent study by Xiao et al [15] revealed that there are 26 stable 2D binary alloys in which their components are from elements of group-VA, including P, As, Bi, and Sb. Based on their results, all of these nanostructures are semiconductors with band gap ranging from 0.06 eV to 2.52 eV. Further studies show that group-VA alloys can have tailored properties compared to their single element counterparts [17–20]. For example, charge mobility of the  $\alpha$ -AsP monolayer is about three times higher than that of  $\alpha$ -P [17,18], but its thermal conductivity is lower than single element  $\alpha$ -P [20], very intriguing for thermoelectric devices. Also, the thermal conductivity of the  $\beta$ -SbAs monolayer is reported to be lower than both Sb and As monolayers [19]. The underlying reason is attributed to a lower phonon lifetime of  $\beta$ -SbAs compared to Sb and As.

Very recently, *ab initio* theoretical studies show that 2D binary  $\beta$ -NX (X=P, As, Sb, Bi) compounds with N being nitrogen are also stable in different phases such as  $\beta$ ,  $\alpha$  and  $\delta$  [21,22]. In addition, Ma et al [22] proposed a possible growth of  $\beta$ - and  $\alpha$ -PN on Ag(111) and Ag(110) substrates using the CVD method which can accelerate the prospective experimental studies on

$\beta$ -NX (X=P, As, Sb, Bi) 2D nanosheets. It is also reported that  $\beta$ -NX (X=P, As, Sb, Bi) monolayers can display direct band gap in the  $\delta$ -phase, while they exhibit indirect band gap in the  $\beta$ - and  $\alpha$ -phases [21]. The band gap can be highly tuned by mechanical in-plane strain [22], or point defects [23]. Regarding their mechanical properties, in some phases they show a negative Poisson's ratio (NPR) [21], which results in features such as enhanced sound and vibration absorption, along with high indentation resistance and fracture toughness [24]. These properties allow novel  $\beta$ -NX (X=P, As, Sb, Bi) 2D compounds to have additional applications compared to conventional 2D materials in different industries such as aerospace [25] and medicine [26]. However, to fulfill these potential applications, having a comprehensive description of the thermal properties and phonon transport in NX (X=P, As, Sb, Bi) 2D materials is of paramount importance, which to the best of our knowledge is missing. Thus, in this study we conduct a systematic first-principles study on the thermal properties of the first three members of this family with a buckled structure; including  $\beta$ -NP,  $\beta$ -NAs and  $\beta$ -NSb. The  $\beta$ -phase is chosen as its small lattice-misfit with the Ag substrate [22] can result in higher experimental realization chance. Particularly, we are interested in the questions such as: How does thermal conductivity of  $\beta$ -NX (X=P, As, Sb) compared with its single element counterpart,  $\beta$ -X? What are the relationships between thermal conductivity variation and different factors such as vibrational properties, average atomic mass, and anharmonicity of the lattice? This study aims to further our understanding of phonon transport in 2D materials, specifically 2D alloys. After this introduction the rest of this paper is organized as follows: Section 2 discusses the computational approach and details of the DFT simulations, Section 3 presents our main results and discussions. Finally, Section 4 summarizes the main findings.

## 2- Computational Approach

We solve the PBTE using an iterative self-consistent approach as implemented in the *ShengBTE* package [27–29]. Within this methodology, the only required inputs are the sets of harmonic (second-order) and anharmonic (third-order) interatomic force constants (IFCs), which are obtained from DFT calculations. Having sets of IFCs, the thermal conductivity along the  $\alpha$  direction can be written as

$$k_{\alpha\alpha} = \frac{1}{k_B T^2 A h N} \sum_{\lambda(\mathbf{k}, p)} n_{\lambda}^0 (n_{\lambda}^0 + 1) (\hbar \omega_{\lambda})^2 v_{\lambda}^{\alpha} v_{\lambda}^{\alpha} \tau_{\lambda} , \quad (1)$$

where  $\lambda(\mathbf{k}, p)$  denotes a phonon mode with  $\mathbf{k}$  being the wave vector and  $p$  the phonon branch number,  $A$  is the unit cell area,  $h$  is the thickness of the unit cell,  $\omega$  is the phonon frequency,  $N$  is the number of  $\mathbf{q}$  points in the first Brillouin zone (BZ) for a  $\Gamma$ -centered regular grid,  $T$  represents the temperature,  $v_{\lambda}^{\alpha}$  is the phonon group velocity in the direction  $\alpha$ ,  $n_{\lambda}^0$  is the phonon occupation number given by the Bose-Einstein distribution. Also,  $\tau_{\lambda}$  is the phonon lifetime considering the three-phonon scattering process, given by

$$\frac{1}{\tau_{\lambda}} = \frac{1}{N} (\sum_{\lambda' \lambda''}^{+} \Gamma_{\lambda \lambda' \lambda''}^{+} + \frac{1}{2} \sum_{\lambda' \lambda''}^{-} \Gamma_{\lambda \lambda' \lambda''}^{-}), \quad (2)$$

where  $\Gamma_{\lambda \lambda' \lambda''}^{+}$  and  $\Gamma_{\lambda \lambda' \lambda''}^{-}$  are the scattering rates for the absorption and emission three-phonon scattering process, respectively.

First, the 2-atom primitive unit cell of all 2D nanostructures explored here were optimized using the QUANTUM ESPRESSO package [30] to obtain the relaxed lattice parameters (shown in Figure

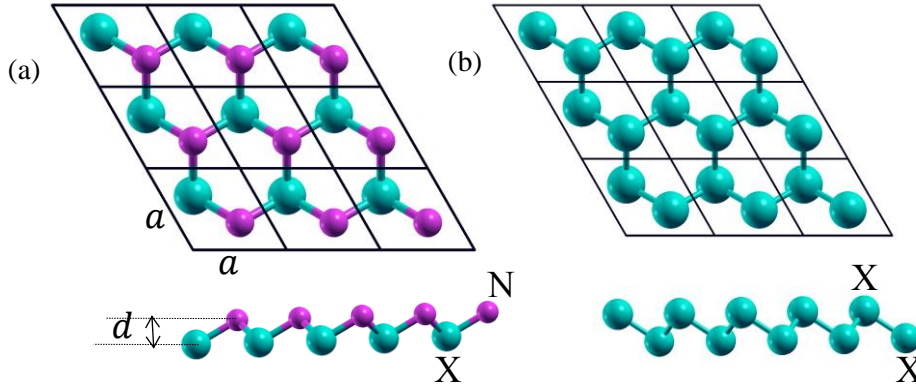


**Fig. 1.** Top and side view of monolayer (a)  $\beta$ -NX ( $X=P, As, Sb$ ), and (b)  $\beta$ -NX.

1). A Perdew-Burke-Ernzerhof (PBE) exchange-correlation functional with a projected augmented wave (PAW) pseudopotential [31,32] is used for all DFT calculations. The convergence thresholds on total energy and forces were chosen to be  $10^{-11}$  a.u. and  $10^{-10}$  a.u., respectively. We used an electronic wave-vector grid of  $31 \times 31 \times 1$  for the Brillouin zone ( $BZ$ ) sampling. The plane-wave energy cutoff is set to a high value of 80Ry. The relaxed lattice parameters obtained from structural optimization are summarized in Table 1. Excellent agreement exists between our results and previously reported values [21,22]. A fine phonon wave-vector grid of  $35 \times 35 \times 1$  is used for the phonon calculation. For the anharmonic calculations, we used the *thirdorder.py* script [27] to generate a set of  $5 \times 5 \times 1$  displaced supercell configurations, with interactions considered up to the tenth nearest neighbor. A  $\Gamma$ -centered Monkhorst-Pack [33] electronic wave-vector grid of  $5 \times 5 \times 1$  is also used for integration over the  $BZ$  of the supercells. Finally, a  $\mathbf{q}$  grid mesh of  $80 \times 80 \times 1$  is adopted for thermal conductivity and other related phonon properties calculations.

Based on Eq. (1) the thermal conductivity of a 2D system depends on its thickness,  $h$ . However, this value is ill-defined in these systems [34,35]. To have a fair comparison between different monolayers, we consider the length of the unit cell along the  $z$ -direction ( $h = 20 \text{ \AA}$ ) as the

thickness of the system. Considering this length as the thickness was also suggested in [34] and [36]. For comparisons with other works, one can use the concept of thermal sheet conductance  $G_s$  as  $G_s = k \cdot h$  [35].

Table 1. Average atomic mass ( $\bar{M}$ ), lattice constant ( $a$ ), buckling distance ( $d$ ), scaled a-o gap, mode contribution in thermal conductivity, and thermal sheet conductance ( $G_s$ ) for each system.

Name	$\bar{M}(amu)$	$a(\text{\AA})$	$d(\text{\AA})$	Scaled a-o gap (THz)	%ZA	%TA	%LA	%Optical	$G_s(WK^{-1})$
NP	22.49	2.73	0.86	0.40	37	27	35	1	572.3
P	30.97	3.28	1.24	0.62	57	23	17	3	518.7
NAs	44.46	2.98	0.97	0.94	29	24	46	1	769.2
As	74.92	3.61	1.39	0.81	55	22	19	4	141.4
NSb	67.88	3.28	1.02	1.28	39	25	34	2	693.2
Sb	121.76	4.11	1.64	1.17	42	27	25	6	20.4

## 3- Results and discussion

### 3.1- Thermal conductivity

The calculated thermal conductivities obtained from the iterative solution of the PBTE in a temperature range from 200K to 800K are plotted in Figure 2. Also, the room temperature thermal sheet conductances [35] are listed in Table 1. All results correspond to monolayers with the same thickness of 20Å. First, we confirm that our prediction of the room temperature thermal sheet

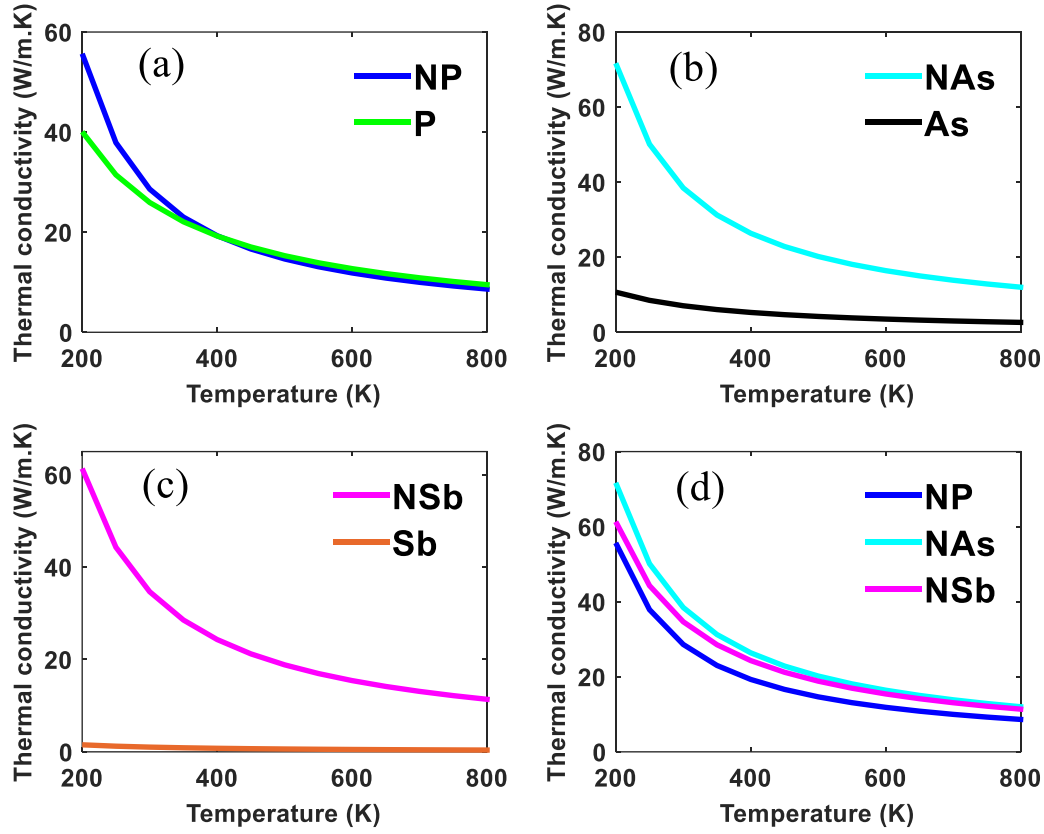


**Fig. 2.** Temperature variation thermal conductivity in 20Å thick layers of (a)  $\beta$ -NP and  $\beta$ -P, (b)  $\beta$ -NAs and  $\beta$ -As, (c)  $\beta$ -NSb and  $\beta$ -Sb, and (d)  $\beta$ -NP,  $\beta$ -NAs and  $\beta$ -NSb.

conductances of P, As and Sb monolayers are in fair accordance with previously reported values [11,12,37], which verifies our workflow in this study. Figures 2(a)-2(c) compare the lattice thermal conductivity of  $\beta$ -NX (X=P, As, Sb) with its single element pristine counterpart,  $\beta$ -X. As can be seen from Figure 2(a), at lower temperatures including room temperature, monolayer NP has higher thermal conductivity in comparison with  $\beta$ -P. However, for temperatures higher than 400K, it can be seen that  $\beta$ -NP and  $\beta$ -P have almost the same thermal conductivities. Guo and Dong [38] studied the lattice thermal conductivity of  $\beta$ -AsP alloy monolayer, and they also found that  $\beta$ -AsP has a similar thermal conductivity as one of its single element counterparts,  $\beta$ -As.



Based on Figure 2(b), monolayer  $\beta$ -NAs has higher thermal conductivity than  $\beta$ -As over the entire temperature range. For example, at room temperature the thermal conductivity of  $\beta$ -NAs (38.46 W/m.K) is about 5.5 times higher than that of monolayer  $\beta$ -As (7.07 W/m.K). Similarly, from Figure 2(c) it can be seen that  $\beta$ -NSb has much higher thermal conductivity compared to  $\beta$ -Sb over the entire temperature range. We find that the room temperature thermal conductivity of 20Å thick layer  $\beta$ -NSb is 34.66 W/m.K, almost 34.0 times higher than that of  $\beta$ -Sb, 1.02 W/m.K. Thus, due to higher thermal conductivity, monolayers  $\beta$ -NAs and  $\beta$ -NSb can be better candidates for thermal management applications compared to their single element counterparts,  $\beta$ -As and  $\beta$ -Sb. Finally, to have a better comparison between different alloys we plot thermal conductivity of  $\beta$ -NP,  $\beta$ -NAs and  $\beta$ -NSb in Figure 2(d). Our results show that  $\beta$ -NAs and  $\beta$ -NP have the highest and lowest thermal conductivity over the considered temperature range, respectively. Interestingly, this is in contrast with the general expectation that monolayers with lower average atomic mass typically have higher thermal conductivities. Similar behavior is also observed in the lattice thermal conductivity of  $\text{La}_3\text{Cu}_3\text{X}_4$  ( $\text{X} = \text{P, As, Sb, Bi}$ ) compounds reported by Pandey et al [39]. Based on their result,  $\text{La}_3\text{Cu}_3\text{P}_4$  has the lowest thermal conductivity compared to other compounds, whereas it is the lightest mass system. In a recent study on the variation of the thermal conductivity ( $k_l$ ) with the average unit cell atomic mass ( $\bar{M}$ ) in group-VA compound monolayers with the puckered structure [40], a relation of the form  $k_l = c_1 + \frac{c_2}{\bar{M}^2}$  is suggested for the thermal conductivity in both Zigzag and Armchair directions. Based on our results shown in Figure 3, we do not find a similar trend between  $k_l$  and  $\bar{M}$  in buckled monolayers of group-VA. However, to better judge the variation of the thermal conductivity with the average atomic mass in buckled group-VA monolayers, analyzing more data points is essential which is outside of the main purpose of this study.

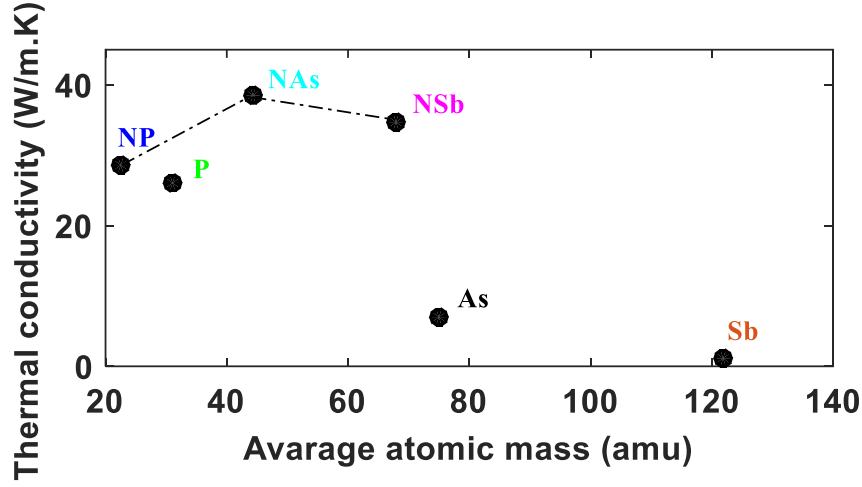


**Fig. 3.** Thermal conductivity versus average atomic mass of unit cell for  $\beta$ -NX (X=P, As, Sb) and  $\beta$ -X monolayers.

Figure 4 shows the contribution of each phonon mode to the total thermal conductivity of  $\beta$ -NX (X=P, As, Sb) and  $\beta$ -X monolayers. As can be seen, for all monolayers except  $\beta$ -NAs, the ZA mode has the highest contribution towards the thermal conductivity. Also, we emphasize that the contribution of the ZA mode is generally higher in  $\beta$ -NX (X=P, As, Sb) than  $\beta$ -X. For instance, the contribution of the ZA, TA and LA modes in  $\beta$ -NP ( $\beta$ -P) are about 37(57) %, 27(23) % and 35(17) %, respectively. Our results are in agreement with Jain and McGaughey's findings which report the dominance of the ZA mode in the thermal conductivity of  $\beta$ -P using the iterative solution of the PBTE [11]. However, it is worth mentioning that although the ZA mode is the dominant heat carrier in these monolayers (except  $\beta$ -NAs), its contribution is much lower than that of graphene, in which the ZA mode contributes to about 80% of the total thermal conductivity [41]. This extremely high contribution in graphene stems from the flat structure and the out-of-plane reflectional symmetry [42], which does not exist in group-VA monolayers and their alloys. Considering  $\beta$ -NAs, the LA mode contributes most to the phonon thermal transport, with a

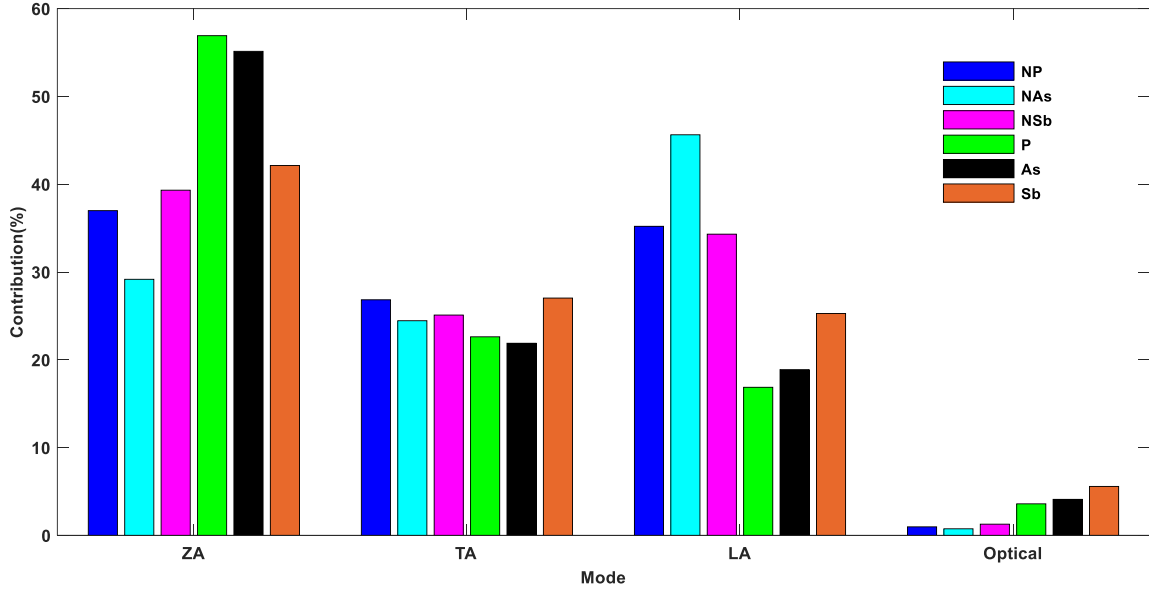


**Fig. 4.** Contribution of each phonon mode towards the total thermal conductivity in  $\beta$ -NX (X=P, As, Sb) and  $\beta$ -X monolayers.

contribution of about 46% in the total thermal conductivity. Also, we find that in all monolayers the optical modes have negligible contribution compared to the acoustic modes. The maximum contribution of the optical modes occurs in  $\beta$ -NSb, which still is only about 6%. This low contribution of the optical modes is usually attributed to the low group velocities and phonon lifetimes of the optical modes.

In order to shed light into the underlying reasons of findings discussed here, different harmonic and anharmonic phonon properties will be studied in details in the next subsections.

### 3.2- Harmonic properties

Figure 5 shows the phonon dispersion curve of  $\beta$ -NX (X=P, As, Sb) along with its single element counterpart  $\beta$ -X. Since all of these monolayers are two atoms per unit cell, the phonon dispersion

curves consist of three acoustic and three optical branches. The out-of-plane acoustic, the in-plane transversal acoustic, and the in-plane longitudinal acoustic modes are labeled as ZA, TA and LA, respectively. It is important to note that as opposed to graphene which has a flat structure, all monolayer studies here have a buckling distance ( $d$ ), which results in the coupling of the ZA mode with the TA and LA modes. Nevertheless, we still use ZA to show the out-of-plane acoustic mode here. In the long-wavelength limit, the ZA branch of all monolayers shows a quadratic behavior which is a typical feature of 2D materials [43,44], while the two other acoustic modes are linear in the same limit.

First, we confirm that there is no imaginary frequency observed in the ZA branch of the dispersion curves, showing that all monolayers considered here are dynamically stable. However, we emphasize that for  $\beta$ -NX (X=P, As, Sb) alloys, a finer phonon wave-vector grid may be required to remove all small negative frequencies near the  $\Gamma$ -point. In our case, a phonon wave-vector grid of  $35 \times 35 \times 1$  works well to remove the “U”-shape negative frequencies zone near the  $\Gamma$ -point. It can be seen from Figure 5 that  $\beta$ -NX (X=P, As, Sb) has generally stiffer acoustic phonons compared to  $\beta$ -X. This results in higher acoustic group velocities for  $\beta$ -NX (X=P, As, Sb) than  $\beta$ -X which will be discussed later. Also, the optical phonons move upwards in  $\beta$ -NX (X=P, As, Sb) compared to  $\beta$ -X, as a result of lower average atomic mass of the unit cell in  $\beta$ -NX (X=P, As, Sb) than to  $\beta$ -X. Phonon dispersion curves of  $\beta$ -AsP and  $\beta$ -As show similar differences as discussed in Ref. [38]. The phonon band gap between the optical and acoustic modes (a-o gap) is an important property which can affect the thermal conductivity by affecting the three-phonon intrinsic processes which both acoustic and optical modes are involved in (such as  $A + A \rightarrow O$ ). The scaled a-o gaps (The a-o gap divided by the maximum acoustic frequency) are listed in Table 1 which are in excellent agreement with previously reported values [37]. As can be seen from

Table 1,  $\beta$ -NAs and  $\beta$ -NSb have higher scaled gap compared to their single element counterparts ( $\beta$ -As and  $\beta$ -Sb) while  $\beta$ -NP has lower scaled gap than  $\beta$ -P. It is worth mentioning that for single element monolayer  $\beta$ -X, the a-o gap is a consequence of the violation of the reflection symmetry. However, two factors of mass difference between constitute atoms along with the violation of the reflection symmetry are responsible for the a-o gap in  $\beta$ -NX (X=P, As, Sb) monolayers.

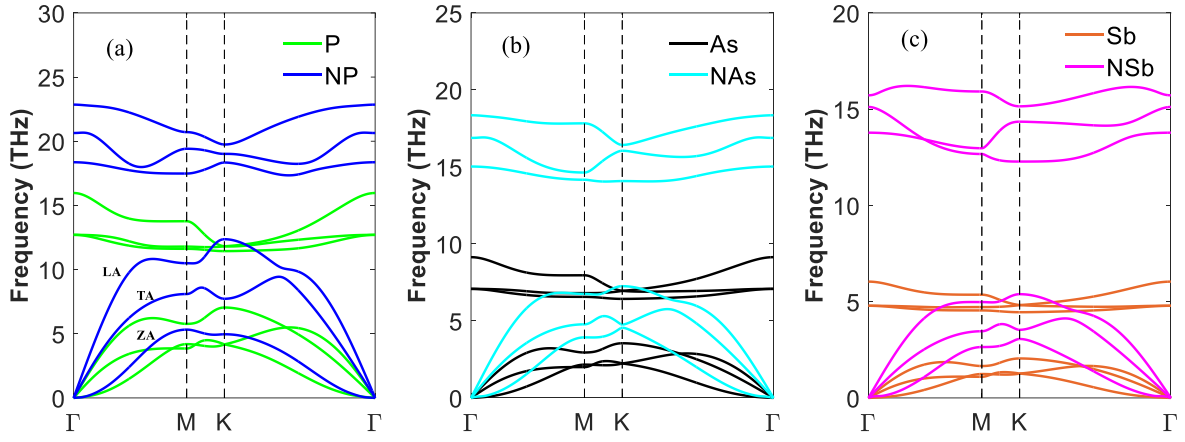
Phonon group velocity as appeared in Eq. (1) is a key parameter in determining the thermal conductivity of a system. Figures 6(a)-6(i) compare the group velocities of  $\beta$ -NX (X=P, As, Sb) to its single element monolayer,  $\beta$ -X. In addition, Figures 6(j)-6(l) show a comparison between group velocity of  $\beta$ -NP,  $\beta$ -NAs, and  $\beta$ -NSb. Due to negligible contribution of the optical phonons toward the total thermal conductivity we only consider acoustic modes here. Based on Figures 6(a)-6(i), it can be seen that generally for all acoustic phonon modes including ZA, TA and LA, monolayer  $\beta$ -NX (X=P, As, Sb) has a higher group velocity than the single element  $\beta$ -X monolayer. This result is consistent with our discussion earlier about the stiffing of the acoustic modes in  $\beta$ -NX (X=P, As, Sb) relative to  $\beta$ -X. For instance, in case of  $\beta$ -NAs ( $\beta$ -NSb) the maximum group velocities of the ZA, TA and LA modes are 3.19 (2.52) km/s, 6.03 (4.94) km/s and 11.68 (9.92) km/s, respectively. The corresponding values for the ZA, TA and LA group velocities of  $\beta$ -As ( $\beta$ -Sb) are 2.12 (1.39), 3.12 (2.16), 4.86 (3.41), respectively. Comparing these values, we can see that some group velocities in  $\beta$ -NX (X=P, As, Sb) can be up to about three times higher than those of  $\beta$ -X. This increased group velocity of  $\beta$ -NX (X=P, As, Sb) compared to  $\beta$ -X is completely in line with the higher thermal conductivity of the  $\beta$ -NX (X=P, As, Sb) monolayer than  $\beta$ -X observed in Figures 2(a)-2(c). We are also interested in comparing the group velocities of  $\beta$ -NP,  $\beta$ -NAS and  $\beta$ -NP together in order to find the reason of thermal conductivity variation shown in Figure 2(d). As can be seen from Figures 6(j)-6(l), from  $\beta$ -NP to  $\beta$ -NAs to  $\beta$ -

NSb group velocity generally decreases with an increase in average unit cell atomic mass. Such a variation in group velocities implies that the lattice thermal conductivity of these alloys should change as  $k_{\beta\text{-NP}} > k_{\beta\text{-NAs}} > k_{\beta\text{-NSb}}$  which is different from the actual trend ( $k_{\beta\text{-NAs}} > k_{\beta\text{-NSb}} > k_{\beta\text{-NP}}$ ) observed in Figure 2(d). Thus, group velocity by itself cannot describe the up-and-down variation of the lattice thermal conductivity in  $\beta\text{-NX}$  (X=P, As, Sb) 2D compounds with the average atomic mass.

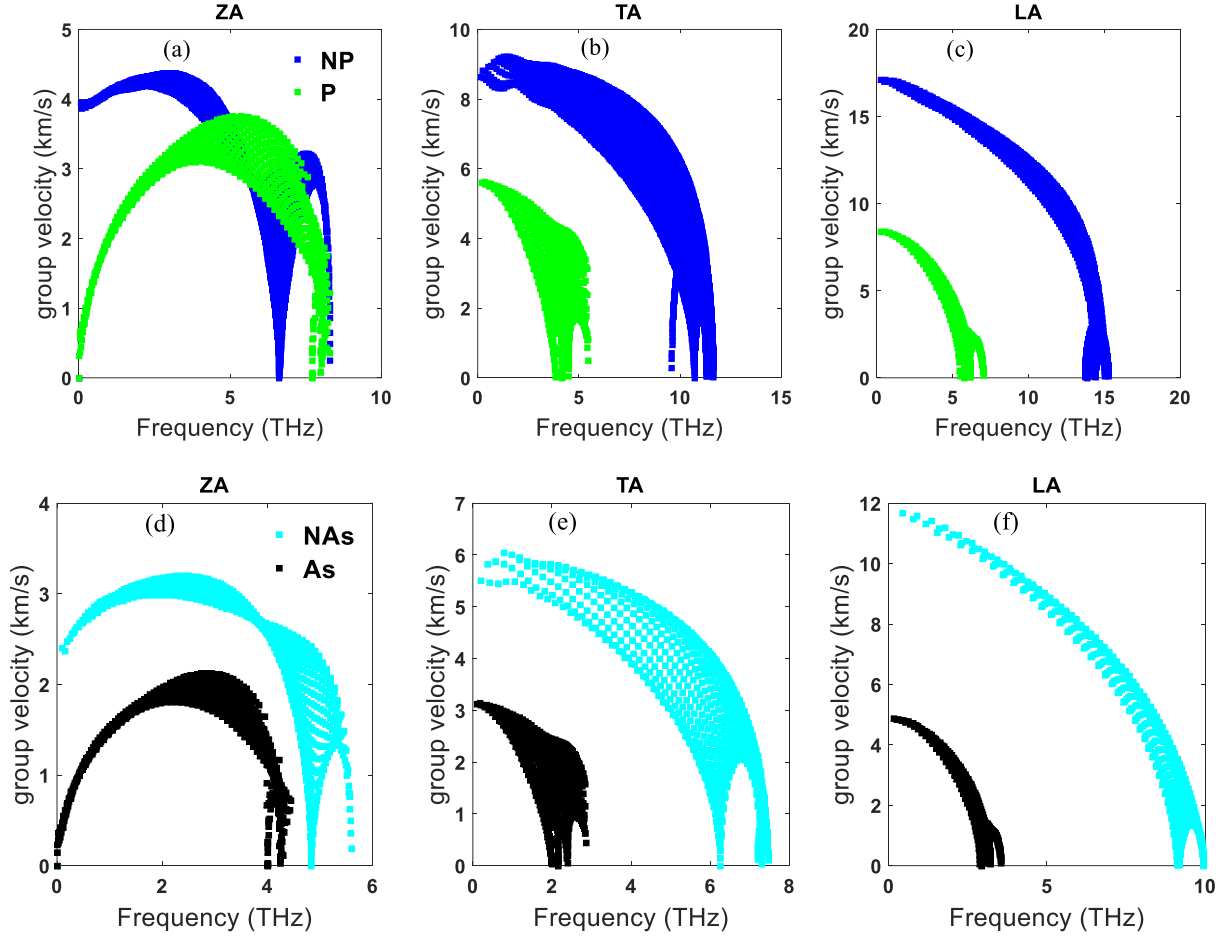
The other important parameter in determining the thermal conductivity of a system which solely depends on harmonic properties is “scattering phase space ( $W$ )” which is a measurement of the space available for the three-phonon process allowed by the conservation of the energy [45]. This parameter is related to phonon frequencies as [45]

$$W_{\lambda}^{\pm} = \frac{1}{2N} \sum_{\lambda' p''} \left\{ \frac{2(n'_0 - n''_0)}{n'_0 + n''_0 + 1} \right\} \frac{\delta(\omega_{\lambda} \pm \omega_{\lambda'} - \omega_{\lambda''})}{\omega_{\lambda} \omega_{\lambda'} \omega_{\lambda''}}, \quad (3)$$

which (+) and (-) correspond to the absorption and emissions processes, respectively. Higher value of  $W$  means that more space is available for the three-phonon scattering processes which typically is an indicator of lower phonon lifetimes and lower thermal conductivity [39,46–48]. Figure 7 shows the scattering phase space of the ZA, TA and LA modes in  $\beta\text{-NX}$  (X=P, As, Sb). Overall, it can be seen that for all phonon modes the phase space increases from  $\beta\text{-NP}$  to  $\beta\text{-NAs}$  to  $\beta\text{-NSb}$ . Due to the inverse correlation between the phase space and the thermal conductivity discussed before, the variation of  $W$  suggests that thermal conductivity changes as  $k_{\beta\text{-NP}} > k_{\beta\text{-NAs}} > k_{\beta\text{-NSb}}$  among  $\beta\text{-NX}$  (X=P, As, Sb) monolayers. However, this trend is not the case based on Figure 2(d) and Figure 3. So, based on our discussion in this subsection, although phonon analysis at the harmonic level can describe the higher thermal conductivity of  $\beta\text{-NX}$  (X=P, As, Sb) compared to  $\beta\text{-X}$ , it fails to interpret the trend observed between  $\beta\text{-NP}$ ,  $\beta\text{-NAs}$  and  $\beta\text{-NSb}$ .



**Fig. 5.** Phonon dispersion curve of (a)  $\beta$ -NP and  $\beta$ -P, (b)  $\beta$ -NAs and  $\beta$ -As, and (c)  $\beta$ -NSb and  $\beta$ -Sb.



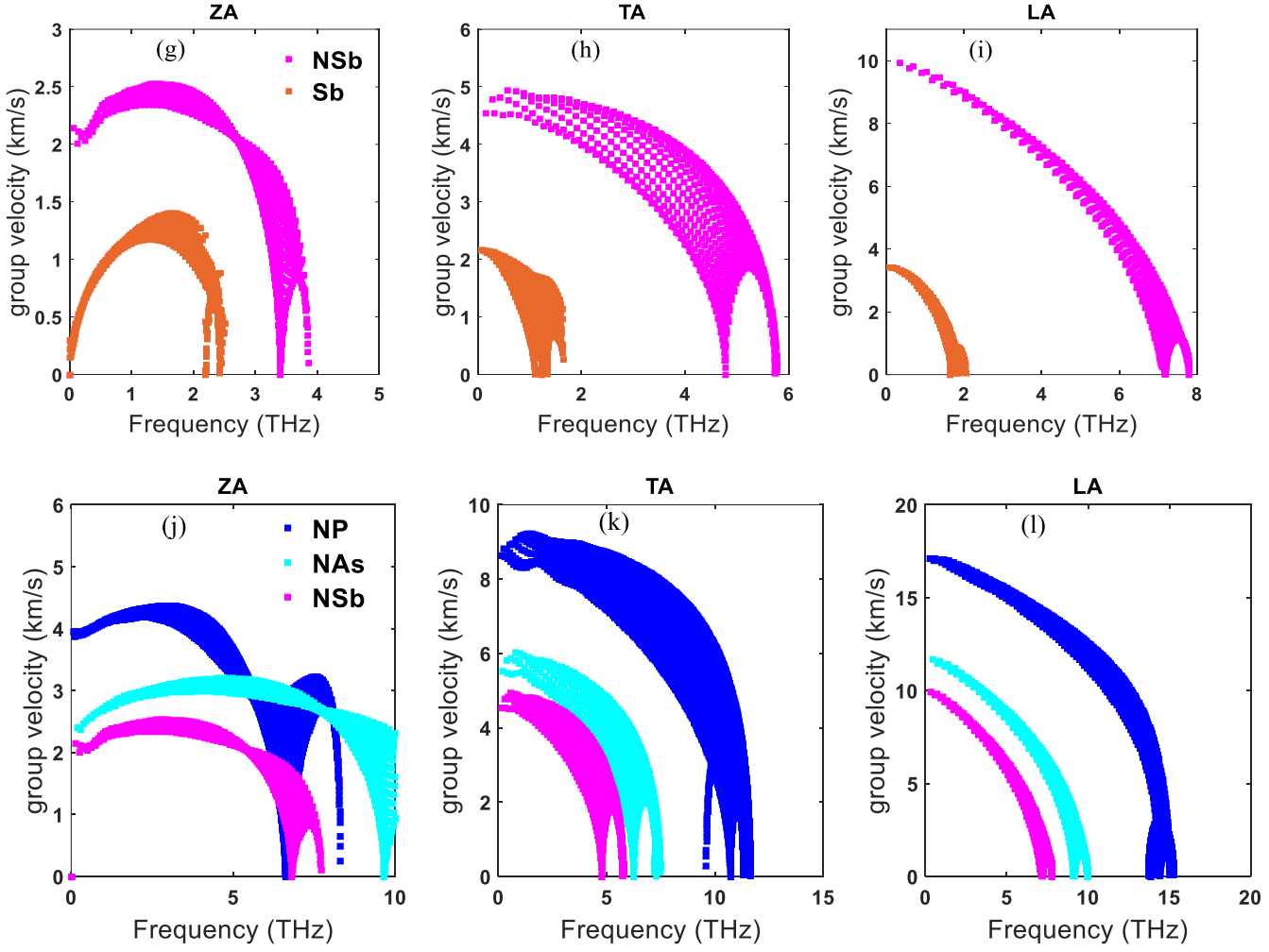


**Fig. 6.** Phonon group velocity of (a) ZA mode in  $\beta$ -NP and  $\beta$ -P, (b) TA mode in  $\beta$ -NP and  $\beta$ -P, (c) LA mode in  $\beta$ -NP and  $\beta$ -P, (d) ZA mode in  $\beta$ -NAs and  $\beta$ -As, (e) TA mode in  $\beta$ -NAs and  $\beta$ -As, (f) LA mode in  $\beta$ -NAs and  $\beta$ -As, (g) ZA mode in  $\beta$ -NSb and  $\beta$ -Sb, (h) TA mode in  $\beta$ -NSb and  $\beta$ -Sb, (i) LA mode in  $\beta$ -NSb and  $\beta$ -Sb, (j) ZA mode in  $\beta$ -NP,  $\beta$ -NAs, and  $\beta$ -NSb, (k) TA mode in  $\beta$ -NP,  $\beta$ -NAs, and  $\beta$ -NSb, and (l) LA mode in  $\beta$ -NP,  $\beta$ -NAs, and  $\beta$ -NSb.



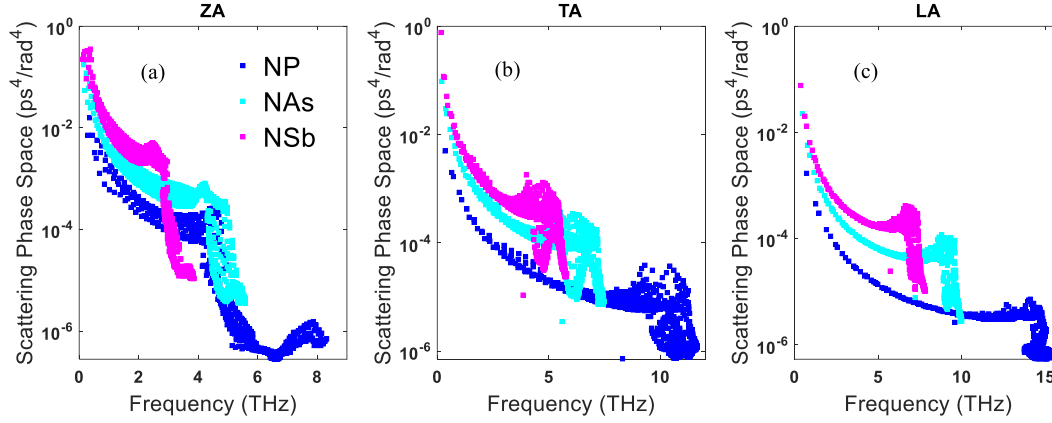


**Fig. 7.** Scattering phase space of the (a)ZA, (b) TA , and (c) LA modes in  $\beta$ -NX (X=P, As, Sb) monolayers.

### 3.3- Phonon lifetime and anharmonic Properties

Figure 8 shows the calculated intrinsic three-phonon lifetimes as a function of frequency at 300K for different acoustic phonon modes. Figures 8(a)-8(i) show a comparison between the phonon lifetime of  $\beta$ -NX (X=P, As, Sb) compound monolayer and its single element counterpart  $\beta$ -X. Also, the three-phonon lifetime of  $\beta$ -NX (X=P, As, Sb) compounds are compared to each other in Figures 8(j)-8(l). Based on Figures 8(a)-8(i), it can be seen that for most of the phonon modes,  $\beta$ -NX (X=P, As, Sb) has higher phonon lifetime than single element  $\beta$ -X. The increased phonon lifetime of  $\beta$ -NX (X=P, As, Sb) relative to  $\beta$ -X is more highlighted at the low frequency region, where the difference between phonon lifetimes can be as high as about four orders of magnitude. The higher phonon lifetime of  $\beta$ -NX (X=P, As, Sb) together with its increased group velocity (See Figure 6), can well describe the higher thermal conductivity of  $\beta$ -NX (X=P, As, Sb) compared to  $\beta$ -X. Figures 8(a)-8(i) aim to compare the phonon lifetimes of  $\beta$ -NX (X=P, As, Sb) compounds together. As can be seen, for most of the phonon modes, phonon lifetimes generally increase from  $\beta$ -NP to  $\beta$ -NAs to  $\beta$ -NSb. Considering the LA mode, we find that at the low frequency region,

$\beta$ -NAs has the highest phonon lifetime. However, at higher frequencies  $\beta$ -NAs and  $\beta$ -NSb have approximately similar LA phonon lifetimes, and  $\beta$ -NP has the lowest. The trends we observed here for phonon lifetimes are similar to those reported for  $\text{La}_3\text{Cu}_3\text{X}_4$  ( $\text{X} = \text{P}, \text{As}, \text{Sb}, \text{Bi}$ ) compounds [39], which show that the heaviest system ( $\text{La}_3\text{Cu}_3\text{Bi}_4$ ) has the longest lifetime, whereas the lightest system ( $\text{La}_3\text{Cu}_3\text{P}_4$ ) has the shortest. There are two important factors in determining the phonon lifetime of a system: 1- scattering phase space, and 2- system anharmonicity. Based on Figure 7 and our discussion in subsection 3.2,  $\beta$ -NP has the minimum phase space available for the three phonon scattering processes and  $\beta$ -NSb has the highest one. This will give rise to larger phonon lifetimes for  $\beta$ -NP compared to  $\beta$ -NAs and  $\beta$ -NSb. So, exploring the scattering phase space is not enough to understand the underlying reason of the trend we observed for the lifetimes of  $\beta$ -NX ( $\text{X} = \text{P}, \text{As}, \text{Sb}$ ) monolayers. System anharmonicity, which determines the strength of three-phonon scattering process is the key feature that remains to be analyzed. A system with higher anharmonicity has stronger phonon-phonon interactions which give rise to lower phonon lifetime and thermal conductivity. The Grüneisen parameters ( $\gamma_\lambda$ ) [49] is usually used as a measurement of the anharmonicity of a structure. This parameter relates to the anharmonic IFCs by

$$\gamma_\lambda = -\frac{1}{6\omega_\lambda^2} \sum_{ijk\alpha\beta\gamma} \frac{\epsilon_{i\alpha}^{\lambda*} \epsilon_{j\beta}^\lambda}{\sqrt{M_i M_j}} r_k^\gamma \Phi_{ijk}^{\alpha\beta\gamma} e^{i\mathbf{k} \cdot \mathbf{r}_j}, \quad (4)$$

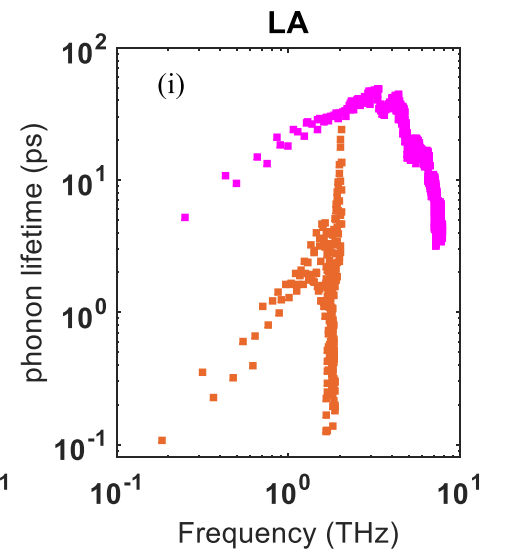
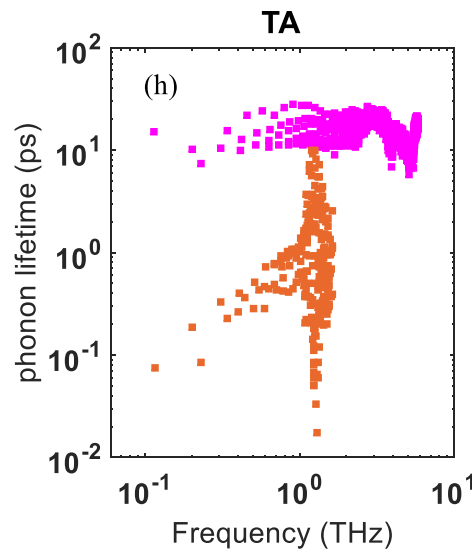
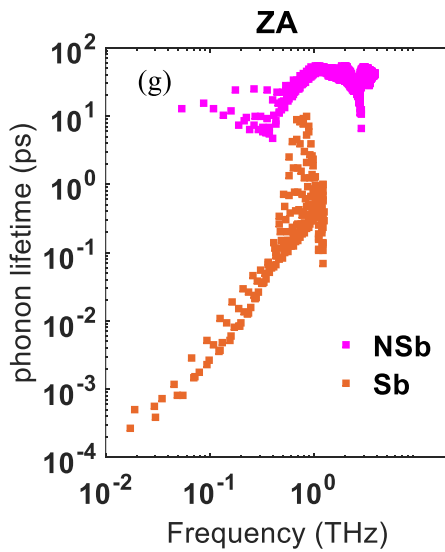
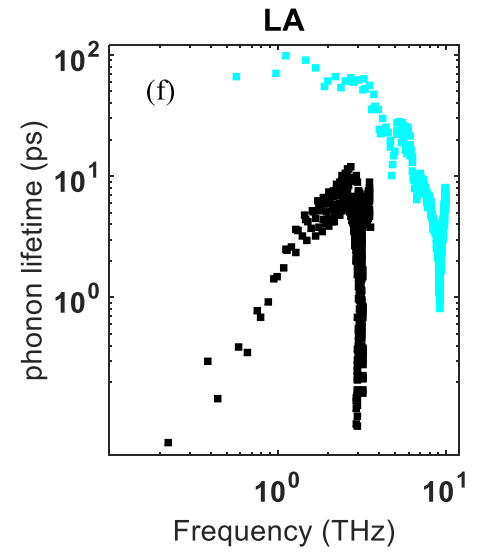
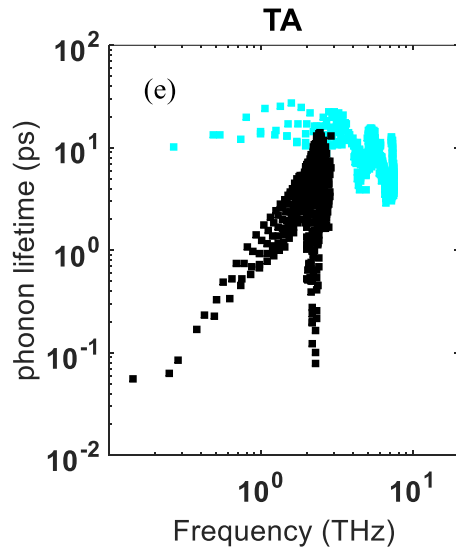
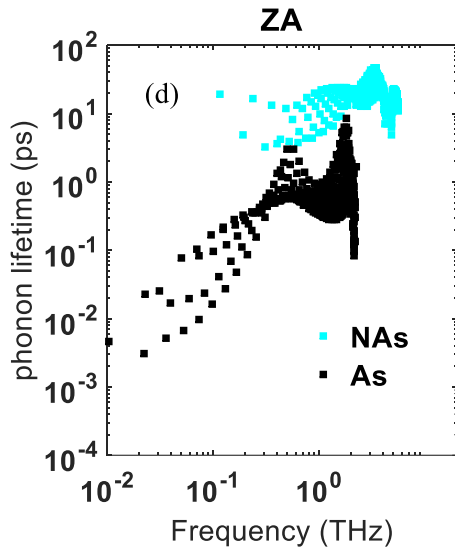
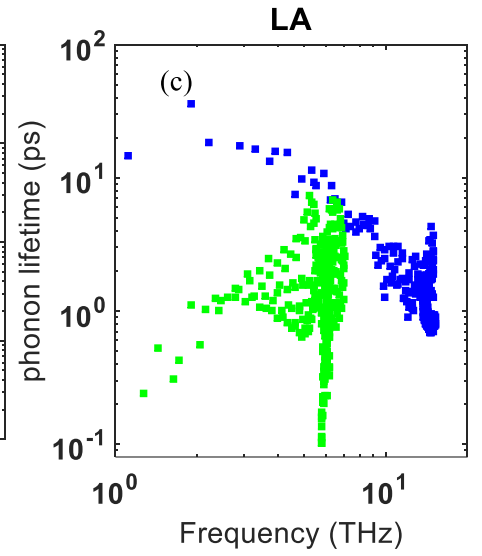
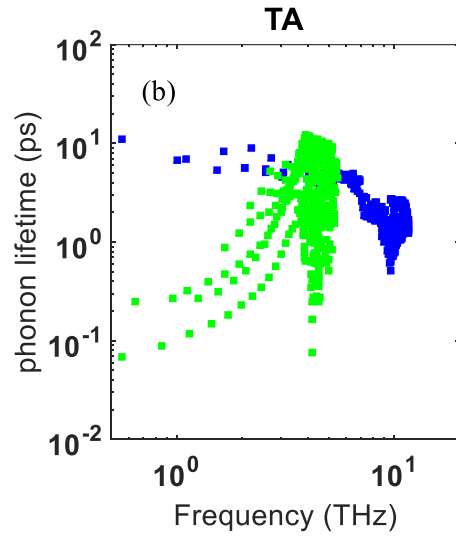
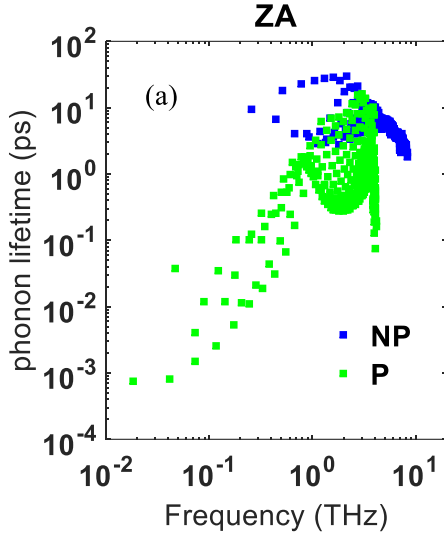
where  $\alpha, \beta$  and  $\gamma$  are the Cartesian components;  $i, j$  and  $k$  denote atomic indices;  $M_i$  represents the mass of atom  $i$ ;  $\epsilon_{i\alpha}^\lambda$  is the phonon eigenvector for atom  $i$  in direction  $\alpha$ ;  $\mathbf{r}_i$  is the position vector of  $i^{\text{th}}$  atom, and finally  $\Phi_{ijk}^{\alpha\beta\gamma}$  represents the third-order anharmonic IFCs. A larger  $\gamma_\lambda$  (magnitude) depicts that the system is more anharmonic which results in a lower thermal conductivity. Figure 9(a) shows the mode-dependent Grüneisen parameters for  $\beta$ -NX ( $\text{X} = \text{P}, \text{As}, \text{Sb}$ ) monolayers. The

inset [Figure 9\(b\)](#) is also focused on the positive values of  $\gamma_\lambda$ . It can be seen that for most of the phonons,  $\beta$ -NP and  $\beta$ -NSb have the highest and lowest Grüneisen parameters, respectively. The trend of  $\gamma_\lambda$  observed here is similar to that in  $\text{La}_3\text{Cu}_3\text{X}_4$  ( $\text{X} = \text{P, As, Sb, Bi}$ ), with  $\text{La}_3\text{Cu}_3\text{P}_4$  and  $\text{La}_3\text{Cu}_3\text{Bi}_4$  possess the highest and the lowest  $\gamma_\lambda$ , respectively. Analyzing the Grüneisen parameters combined with the group velocities and the scattering phase space one can well understand the thermal conductivity variation among the  $\beta$ -NX ( $\text{X}=\text{P, As, Sb}$ ) 2D compounds. There is a competition between harmonic (group velocity and scattering phase space) and anharmonicity of the lattice in determining the thermal conductivity of  $\beta$ -NX ( $\text{X}=\text{P, As, Sb}$ ). Harmonic effects tend to decrease the lattice thermal conductivity from  $\beta$ -NP to  $\beta$ -NAs to  $\beta$ -NSb, while higher anharmonicity in  $\beta$ -NP relative to  $\beta$ -NAs and  $\beta$ -NSb more than compensates the effects of harmonic properties, gives rise to a lower thermal conductivity for  $\beta$ -NP. Considering all these effects results in an up-and-down behavior for the lattice thermal conductivity of  $\beta$ -NP to  $\beta$ -NAs to  $\beta$ -NSb. Interestingly, similar interplays between harmonic and anharmonic properties cause  $\text{La}_3\text{Cu}_3\text{Sb}_4$  to have the highest thermal conductivity between  $\text{La}_3\text{Cu}_3\text{X}_4$  ( $\text{X} = \text{P, As, Sb, Bi}$ ) compounds [\[39\]](#).

### 3.1- Phonon mean free path and size effects

Phonon mean free path (MFP) is an important parameter in designing nanostructures and controlling the lattice thermal conductivity of a system which can practically be measured using the thermal conductivity spectroscopy technique [\[50\]](#). The normalized thermal conductivity accumulation for  $\beta$ -NX ( $\text{X}=\text{P, As, Sb}$ ) 2D compounds as well as single element  $\beta$ -X at 300K are plotted in [Figure 10](#). The normalized thermal conductivity accumulation increases with increasing MPF, and finally converges to one. In order to compare different monolayers, we calculate a

critical MPF at which thermal conductivity has 85% of its saturated value. The values of this critical MPF are 35nm, 109 nm, 191 nm, 429 nm, 660 nm, and 690 nm for  $\beta$ -Sb,  $\beta$ -As,  $\beta$ -P,  $\beta$ -NP,  $\beta$ -NAs, and  $\beta$ -NSb, respectively. It can be seen that critical MPF is much higher for all  $\beta$ -NX (X=P, As, Sb) compounds compared to their single element counterpart which can stem from higher group velocity and phonon lifetime in  $\beta$ -NX (X=P, As, Sb) compounds compared to  $\beta$ -X. This implies that the effects of sample size on thermal conductivity is more important in  $\beta$ -NX (X=P, As, Sb) alloys than single elements group-VA monolayers. Strain engineering is also found to give rise to the size effects in 2D nanostructures [36,51].



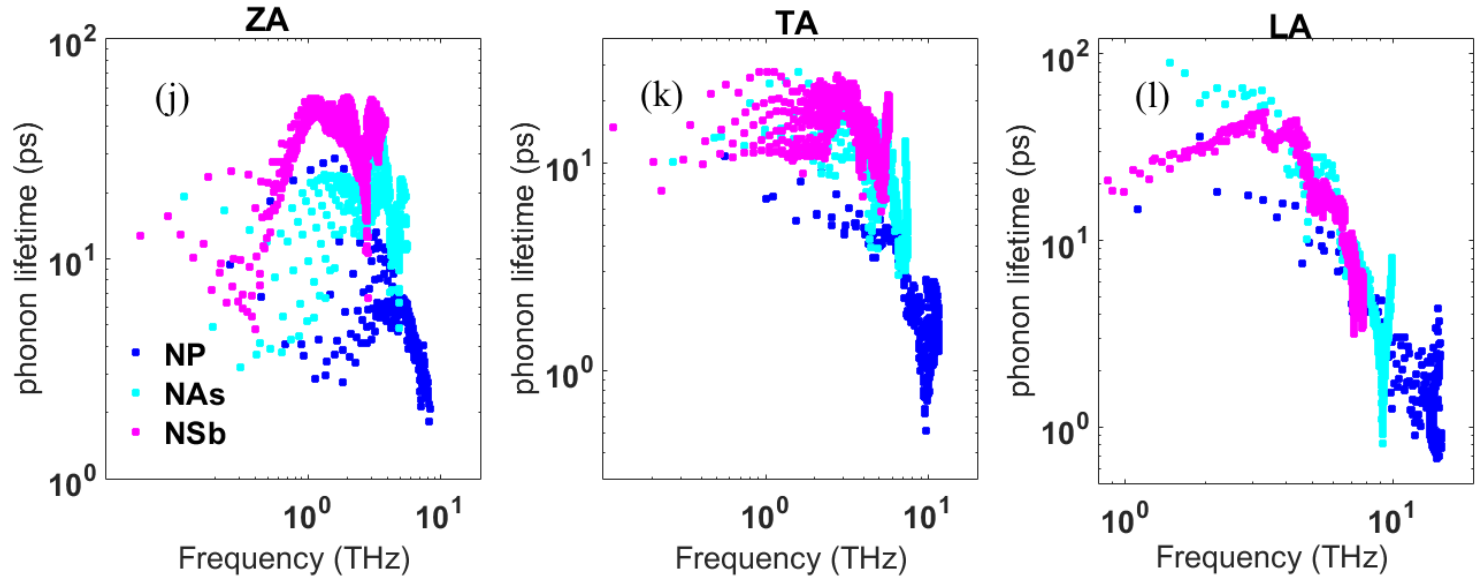


**Fig. 8.** Room temperature Phonon lifetime of (a) ZA mode in  $\beta$ -NP and  $\beta$ -P, (b) TA mode in  $\beta$ -NP and  $\beta$ -P, (c) LA mode in  $\beta$ -NP and  $\beta$ -P, (d) ZA mode in  $\beta$ -NAs and  $\beta$ -As, (e) TA mode in  $\beta$ -NAs and  $\beta$ -As, (f) LA mode in  $\beta$ -NAs and  $\beta$ -As, (g) ZA mode in  $\beta$ -NSb and  $\beta$ -Sb, (h) TA mode in  $\beta$ -NSb and  $\beta$ -Sb, (i) LA mode in  $\beta$ -NSb and  $\beta$ -Sb, (j) ZA mode in  $\beta$ -NP,  $\beta$ -NAs, and  $\beta$ -NSb (k) TA mode in  $\beta$ -NP,  $\beta$ -NAs, and  $\beta$ -NSb, and (l) LA mode in  $\beta$ -NP,  $\beta$ -NAs, and  $\beta$ -NSb.

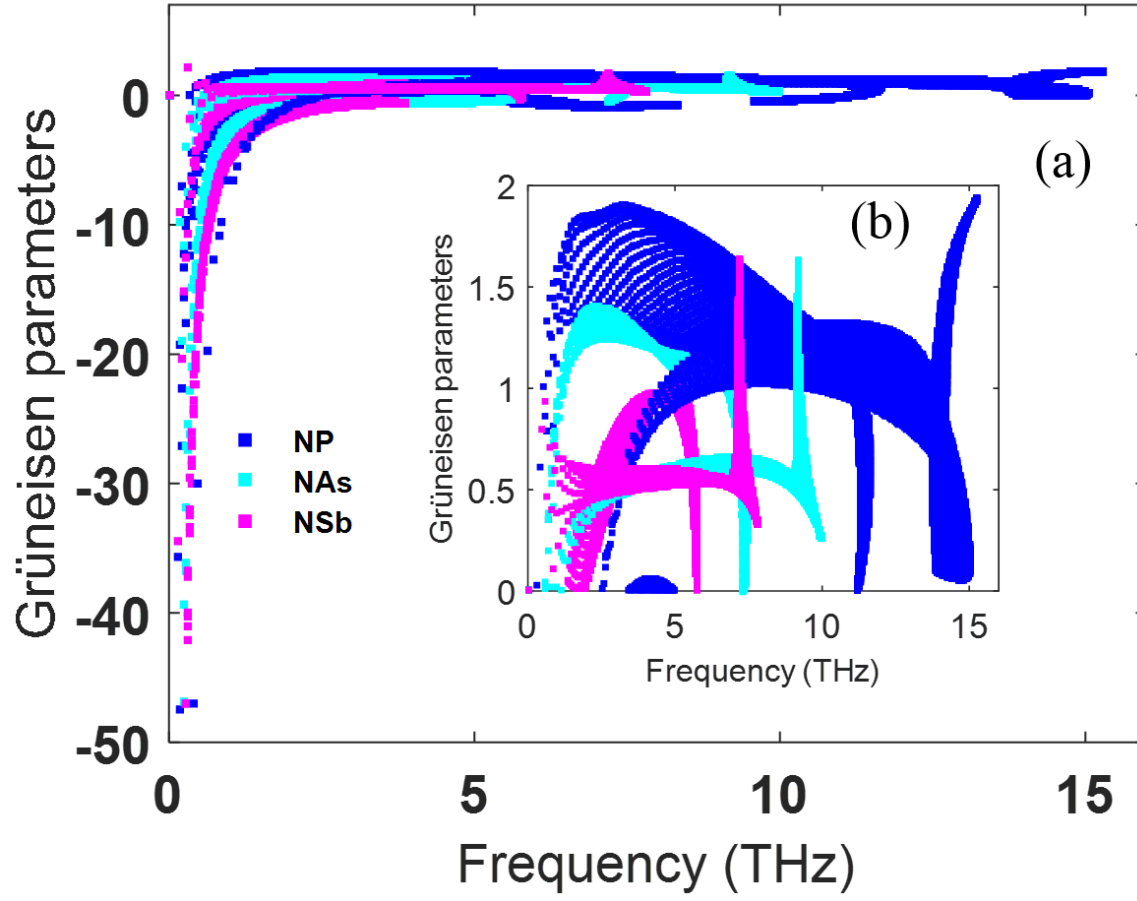


**Fig. 9.** (a) Grüneisen parameters in  $\beta$ -NX (X=P, As, Sb) monolayers (b) Positive values of the Grüneisen parameters.

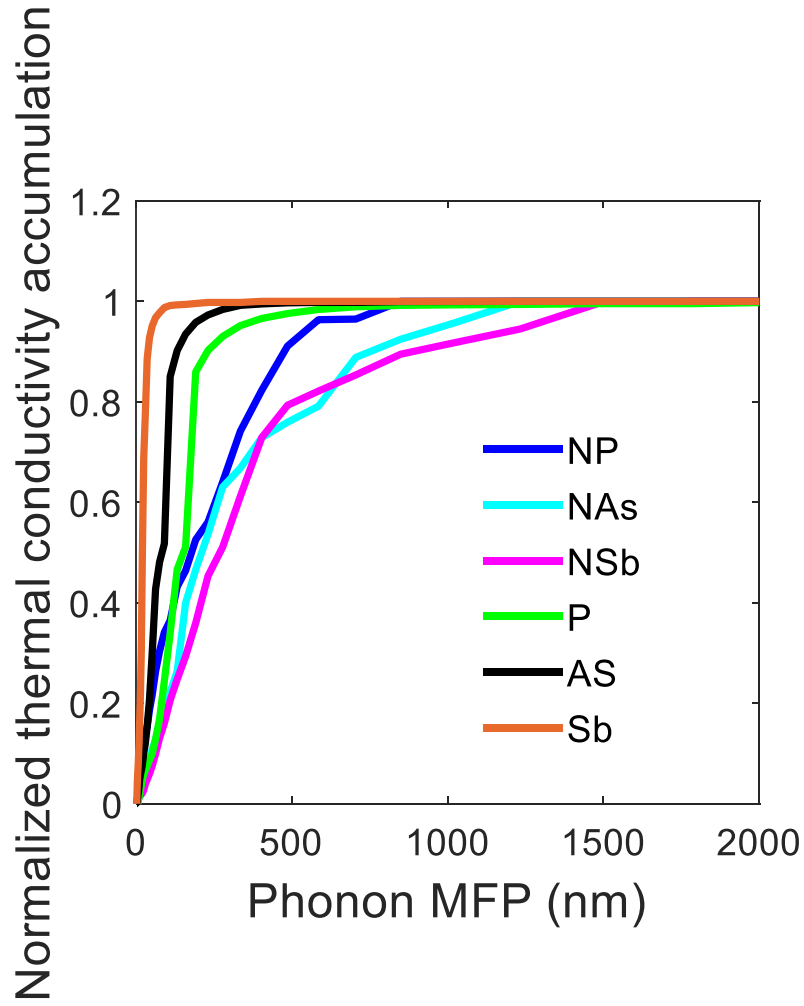


**Fig. 10.** Normalized thermal conductivity accumulation at 300K for  $\beta$ -NX (X=P, As, Sb) and  $\beta$ -X.



## 4-Summary and conclusion

As a summary, we conducted a rigorous first-principles DFT study based on the iterative solution of the PBTE to study phonon thermal transport and thermal conductivity in novel  $\beta$ -NX (X=P, As, Sb) 2D structures. We found that the room temperature thermal conductivity of 20Å thick layers of  $\beta$ -NP,  $\beta$ -NAs and  $\beta$ -NSb are 28.615 W/mK, 38.46 W/mK, and 34.66 W/mK, respectively. For each of these compound monolayers, the room temperature thermal conductivity is higher than its corresponding value in their single elements counterpart,  $\beta$ -P,  $\beta$ -As and  $\beta$ -Sb. The higher thermal conductivity of  $\beta$ -NX (X=P, As, Sb) compared to  $\beta$ -X is attributed to higher phonon lifetime and group velocity in  $\beta$ -NX (X=P, As, Sb) than  $\beta$ -X. Interestingly we found that despite having the lowest average atomic mass,  $\beta$ -NP has the minimum thermal conductivity between  $\beta$ -NX (X=P, As, Sb) compounds. All harmonic properties such as group velocity and scattering phase space failed to clarify the trend of thermal conductivity observed in  $\beta$ -NX (X=P, As, Sb) monolayers. However, analyzing the Grüneisen parameter as a measurement of the strength of anharmonic three-phonon processes shows that  $\beta$ -NP has the highest anharmonicity which leads to lower phonon lifetime and thermal conductivity. The competition between harmonic and anharmonic properties is responsible for an up-and-down variation of the lattice thermal conductivity with average atomic mass in  $\beta$ -NX (X=P, As, Sb) compound monolayers. This paper highlights the importance of having a comprehensive understanding of the interplay between harmonic and anharmonic phonon properties, which can provide useful insights into phonon thermal transport in novel structures.

## Conflicts of interest

There is no conflicts to declare.

## Acknowledgment

This work was supported by the Natural Sciences and Engineering Research Council of Canada (NSERC), through the Discovery and the Collaborative Research and Development (CRD) grant programs. Computations were performed on the GPC supercomputer at the SciNet HPC Consortium. SciNet is funded by the Canada Foundation for Innovation under the auspices of Compute Canada; the Government of Ontario; Ontario Research Fund—Research Excellence; and the University of Toronto.

## References

- [1] Liu H, Neal A T, Zhu Z, Luo Z, Xu X, Tománek D and Ye P D 2014 Phosphorene: An unexplored 2D semiconductor with a high hole mobility *ACS Nano* **8** 4033–41
- [2] Li L, Yu Y, Ye G J, Ge Q, Ou X, Wu H, Feng D, Chen X H and Zhang Y 2014 Black phosphorus field-effect transistors *Nat. Nanotechnol.* **9** 372–7
- [3] Zhang S, Xie M, Li F, Yan Z, Li Y, Kan E, Liu W, Chen Z and Zeng H 2016 Semiconducting Group 15 Monolayers: A Broad Range of Band Gaps and High Carrier Mobilities *Angew. Chemie - Int. Ed.* **55** 1666–9
- [4] Zhang S, Guo S, Chen Z, Wang Y, Gao H, Gómez-Herrero J, Ares P, Zamora F, Zhu Z and Zeng H 2018 Recent progress in 2D group-VA semiconductors: from theory to

- experiment *Chem. Soc. Rev.* **47** 982–1021
- [5] Mardanya S, Thakur V K, Bhowmick S and Agarwal A 2016 Four allotropes of semiconducting layered arsenic that switch into a topological insulator via an electric field: Computational study *Phys. Rev. B* **94** 1–9
- [6] Carrete J, Gallego L J and Mingo N 2017 Structural Complexity and Phonon Physics in 2D Arsenenes *J. Phys. Chem. Lett.* **8** 1375–80
- [7] Mu Y and Si M S 2015 The mechanical exfoliation mechanism of black phosphorus to phosphorene: A first-principles study *Epl* **112**
- [8] Zhang Y, Dong N, Tao H, Yan C, Huang J, Liu T, Robertson A W, Texter J, Wang J and Sun Z 2017 Exfoliation of Stable 2D Black Phosphorus for Device Fabrication *Chem. Mater.* **29** 6445–56
- [9] Smith J B, Hagaman D and Ji H F 2016 Growth of 2D black phosphorus film from chemical vapor deposition *Nanotechnology* **27**
- [10] Zeng J, Cui P and Zhang Z 2017 Half Layer by Half Layer Growth of a Blue Phosphorene Monolayer on a GaN(001) Substrate *Phys. Rev. Lett.* **118** 1–5
- [11] Jain A and McGaughey A J H 2015 Strongly anisotropic in-plane thermal transport in single-layer black phosphorene *Sci. Rep.* **5** 8501
- [12] Zheng G, Jia Y, Gao S and Ke S H 2016 Comparative study of thermal properties of group-VA monolayers with buckled and puckered honeycomb structures *Phys. Rev. B* **94** 1–6
- [13] Zhang D-C, Zhang A-X and Guo S-D 2017 Thermoelectric properties of  $\beta$ -As, Sb

- and Bi monolayers *RSC Adv.* **7** 24537–46
- [14] Zeraati M, Vaez Allaei S M, Abdolhosseini Sarsari I, Pourfath M and Donadio D 2016 Highly anisotropic thermal conductivity of arsenene: An ab initio study *Phys. Rev. B* **93** 1–5
- [15] Xiao W Z, Xiao G, Rong Q Y and Wang L L 2018 New two-dimensional V-V binary compounds with a honeycomb-like structure: A first-principles study *Mater. Res. Express* **5**
- [16] Yu W, Niu C Y, Zhu Z, Wang X and Zhang W B 2016 Atomically thin binary V-V compound semiconductor: A first-principles study *J. Mater. Chem. C* **4** 6581–7
- [17] Xie M, Zhang S, Cai B, Huang Y, Zou Y, Guo B, Gu Y and Zeng H 2016 A promising two-dimensional solar cell donor: Black arsenic–phosphorus monolayer with 1.54 eV direct bandgap and mobility exceeding  $14,000 \text{ cm}^2 \text{ V}^{-1} \text{ s}^{-1}$  *Nano Energy* **28** 433–9
- [18] Shojaei F and Kang H S 2015 Electronic Structure and Carrier Mobility of Two-Dimensional  $\alpha$  Arsenic Phosphide *J. Phys. Chem. C* **119** 20210–6
- [19] Guo S D and Liu J T 2017 Lower lattice thermal conductivity in SbAs than As or Sb monolayers: A first-principles study *Phys. Chem. Chem. Phys.* **19** 31982–8
- [20] Sun Y, Shuai Z and Wang D 2018 Lattice thermal conductivity of monolayer AsP from first-principles molecular dynamics *Phys. Chem. Chem. Phys.* **20** 14024–30
- [21] Xiao W Z, Xiao G, Rong Q Y and Wang L L 2018 Theoretical discovery of novel two-dimensional VA-N binary compounds with auxiticity *Phys. Chem. Chem. Phys.* **20** 22027–37

- [22] Ma S, He C, Sun L Z, Lin H, Li Y and Zhang K W 2015 Stability of two-dimensional PN monolayer sheets and their electronic properties *Phys. Chem. Chem. Phys.* **17** 32009–15
- [23] Benam Z H, Arkin H and Aktürk E 2019 Tuning electronic and magnetic properties of single-layer PN phases by point defects *J. Phys. Chem. Solids* **125** 80–9
- [24] Alderson K L, Pickles A P, Neale P J and Evans K E 1994 Auxetic polyethylene: The effect of a negative poisson's ratio on hardness *Acta Metall. Mater.* **42** 2261–6
- [25] Liu Q 2006 Literature review: materials with negative poisson's ratios and potential applications to Aerospace and Defence *Aust. Gov. Dep. Def.* 1–47
- [26] Scarpa F 2008 Auxetic materials for bioprotheses *IEEE Signal Process. Mag.* **25**
- [27] Li W, Carrete J, Katcho N A and Mingo N 2014 ShengBTE: A solver of the Boltzmann transport equation for phonons *Comput. Phys. Commun.* **185** 1747–58
- [28] Esfarjani K and Stokes H T 2008 Method to extract anharmonic force constants from first principles calculations *Phys. Rev. B - Condens. Matter Mater. Phys.* **77** 1–7
- [29] McGaughey A J H, Jain A and Kim H-Y 2019 Phonon properties and thermal conductivity from first principles, lattice dynamics, and the Boltzmann transport equation *J. Appl. Phys.* **125** 011101
- [30] Giannozzi P, Baroni S, Bonini N, Calandra M, Car R, Cavazzoni C, Ceresoli D, Chiarotti G L, Cococcioni M, Dabo I, Dal Corso A, De Gironcoli S, Fabris S, Fratesi G, Gebauer R, Gerstmann U, Gougoussis C, Kokalj A, Lazzeri M, Martin-Samos L, Marzari N, Mauri F, Mazzarello R, Paolini S, Pasquarello A, Paulatto L, Sbraccia C, Scandolo S, Sclauzero G, Seitsonen A P, Smogunov A, Umari P and Wentzcovitch R M 2009 QUANTUM

- ESPRESSO: A modular and open-source software project for quantum simulations of materials *J. Phys. Condens. Matter* **21**
- [31] Taheri A, Da Silva C and Amon C H 2018 First-principle phonon thermal transport in graphene: Effects of exchange-correlation and type of pseudopotential *J. Appl. Phys.* **123** 215105
- [32] P.E. B 1994 Projector augmented-wave method *Phys. Rev. B* **50** 17953–79
- [33] Pack J D and Monkhorst H J 1977 “special points for Brillouin-zone integrations”-a reply *Phys. Rev. B* **16** 1748–9
- [34] Zhang A-X, Liu J-T and Guo S-D 2017 Strain effects on phonon transport in antimonene from a first-principles study *Phys. Chem. Chem. Phys.* **19** 14520–6
- [35] Wu X, Varshney V, Lee J, Pang Y, Roy A K and Luo T 2017 How to characterize thermal transport capability of 2D materials fairly? – Sheet thermal conductance and the choice of thickness *Chem. Phys. Lett.* **669** 233–7
- [36] Taheri A, Da Silva C and Amon C 2018 Effects of biaxial tensile strain on the first-principles-driven thermal conductivity of buckled arsenene and phosphorene *Phys. Chem. Chem. Phys.* 15–23
- [37] Peng B, Zhang D, Zhang H, Shao H, Ni G, Zhu Y and Zhu H 2017 The conflicting role of buckled structure in phonon transport of 2D group-IV and group-V materials *Nanoscale* **9** 7397–407
- [38] Guo S D and Dong J 2018 Biaxial tensile strain tuned up-and-down behavior on lattice thermal conductivity in  $\beta$ -AsP monolayer *J. Phys. D: Appl. Phys.* **51**

- [39] Pandey T, Polanco C A, Lindsay L and Parker D S 2017 Lattice thermal transport in  $\text{La}_3\text{Cu}_3\text{X}_4$  compounds (X= P, As, Sb, Bi): Interplay of anharmonicity and scattering phase space *Phys. Rev. B* **95** 1–7
- [40] Kocabaş T, Çakir D, Gülseren O, Ay F, Kosku Perkgöz N and Sevik C 2018 A distinct correlation between the vibrational and thermal transport properties of group VA monolayer crystals *Nanoscale* **10** 7803–12
- [41] Kuang Y, Lindsay L, Shi S, Wang X and Huang B 2016 Thermal conductivity of graphene mediated by strain and size *Int. J. Heat Mass Transf.* **101** 772–8
- [42] Lindsay L, Broido D A and Mingo N 2011 Flexural phonons and thermal transport in multilayer graphene and graphite *Phys. Rev. B - Condens. Matter Mater. Phys.* **83** 1–5
- [43] Zabel H 2001 Phonons in layered compounds *J. Phys. Condens. Matter* **13** 7679
- [44] Carrete J, Li W, Lindsay L, Broido D A, Gallego L J and Mingo N 2016 Physically founded phonon dispersions of few-layer materials and the case of borophene *Mater. Res. Lett.* **4** 204–11
- [45] Li W and Mingo N 2015 Ultralow lattice thermal conductivity of the fully filled skutterudite  $\text{YbFe}_4\text{Sb}_{12}$  due to the flat avoided-crossing filler modes *Phys. Rev. B - Condens. Matter Mater. Phys.* **91** 1–6
- [46] Tadano T, Gohda Y and Tsuneyuki S 2015 Impact of rattlers on thermal conductivity of a thermoelectric clathrate: A first-principles study *Phys. Rev. Lett.* **114** 1–5
- [47] Lindsay L 2016 First Principles Peierls-Boltzmann Phonon Thermal Transport: A Topical Review *Nanoscale Microscale Thermophys. Eng.* **20** 67–84

- [48] Pandey T and Singh A K 2016 Simultaneous enhancement of electrical conductivity and thermopower in Bi<sub>2</sub>S<sub>3</sub> under hydrostatic pressure *J. Mater. Chem. C* **4** 1979–87
- [49] Broido D A, Ward A and Mingo N 2005 Lattice thermal conductivity of silicon from empirical interatomic potentials *Phys. Rev. B - Condens. Matter Mater. Phys.* **72** 1–8
- [50] Minnich A J, Johnson J A, Schmidt A J, Esfarjani K, Dresselhaus M S, Nelson K A and Chen G 2011 Thermal conductivity spectroscopy technique to measure phonon mean free paths *Phys. Rev. Lett.* **107** 1–4
- [51] Kuang Y D, Lindsay L, Shi S Q and Zheng G P 2016 Tensile strains give rise to strong size effects for thermal conductivities of silicene, germanene and stanene *Nanoscale* **8** 3760–7